Evaluation of patient specific MR distortion correction schemes for improved target localization accuracy in SRS

Dimitrios Dellios[1], Eleftherios P Pappas[1], Ioannis Seimenis[1], Chryssa Paraskevopoulou[2], Kostas I Lampropoulos[2], Georgia Lymperopoulou[3], Pantelis Karaiskos[1, 2]

[1] Medical Physics Laboratory, Medical School, National and Kapodistrian University of Athens, 115 27 Athens, Greece

[2] Medical Physics and Gamma Knife Department, Hygeia Hospital, 151 23 Marousi, Greece

[3] 1st Department of Radiology, Medical School, National and Kapodistrian University of Athens, 115 28 Athens, Greece

Corresponding author:
Pantelis Karaiskos
Medical Physics Laboratory, Medical School, National and Kapodistrian University of Athens, Mikras Asias 75, 115 27 Goudi, Athens, Greece
phone: +302107462374
e-mail: pkaraisk@med.uoa.gr

Keywords: MRI, spatial distortion, distortion correction, quality assurance, SRS

Running title: Personalized MR distortion correction

This article has been accepted for publication and undergone full peer review but has not been through the copyediting, typesetting, pagination and proofreading process, which may lead to differences between this version and the Version of Record. Please cite this article as doi: 10.1002/MP.14615

Evaluation of patient specific MR distortion correction schemes for improved target localization accuracy in SRS

Abstract

Purpose: This work aims at promoting target localization accuracy in cranial stereotactic radiosurgery (SRS) applications by focusing on the correction of sequence dependent (also patient induced) Magnetic Resonance (MR) distortions at the lesion locations. A phantom-based quality assurance (QA) methodology was developed and implemented for the evaluation of three distortion correction techniques. The same approach was also adapted to cranial MR images used for SRS treatment planning purposes in single or multiple brain metastases cases.

Methods: A 3D-printed head phantom was filled with a 3D polymer gel dosimeter. Following treatment planning and dose delivery, volumes of radiation-induced polymerization served as hypothetical lesions, offering adequate MR contrast with respect to the surrounding unirradiated areas. T1-weighted (T1w) MR imaging was performed at 1.5T using the clinical scanning protocol for SRS. Additional images were acquired to implement three distortion correction methods; the field mapping (FM), mean image (MI) and signal integration (SI) techniques. Reference lesion locations were calculated as the averaged centroid positions of each target identified in the forward and reverse read gradient polarity MRI scans. The same techniques and workflows were implemented for the correction of contrast enhanced T1w MR images of 10 patients with a total of 27 brain metastases.

Results: All methods employed in the phantom study diminished spatial distortion. Median and maximum distortion magnitude decreased from 0.7 mm (2.10 ppm) and 0.8 mm (2.36 ppm), respectively, to <0.2 mm (0.61 ppm) at all target locations, using any of the three techniques. Image quality of the corrected images was acceptable, while contrast-to-noise ratio slightly increased. Results of the patient study were in accordance to the findings of the phantom study. Residual distortion in corrected patient images was found to be less than 0.3 mm in the vast majority of targets. Overall, the MI approach appears to be the most efficient correction method from the three investigated.

Conclusions: In cranial SRS applications, patient specific distortion correction at the target location(s) is feasible and effective, despite the expense of longer imaging time since additional

MRI scan(s) need to be performed. A phantom-based QA methodology was developed and presented to reassure efficient implementation of correction techniques for sequence dependent spatial distortion.

1. INTRODUCTION

Modern radiotherapy applications greatly benefit from the superior soft tissue contrast capabilities of Magnetic Resonance Images (MRIs) which are, therefore, routinely employed in treatment planning, either along with Computed Tomography (CT) images or as the sole imaging modality. In both cases, the inherent geometric distortions constitute a major drawback for employing MRI in contemporary radiotherapy applications.[1–3] The corresponding dosimetric impact is expected to be more significant in techniques involving steep dose gradients and demanding high dose conformality to the target, such as in cranial Stereotactic Radiosurgery (SRS) treatments. Moreover, the employment of margins for Planning Target Volume (PTV) determination in SRS should be restricted, since it has been associated with increased risk for radiation-induced toxicity.[4–6] Consequently, spatial accuracy in target localization is of paramount importance. Especially in cases involving small brain lesions, an overall spatial offset of the order of 1 mm could considerably compromise SRS treatment efficiency.[7–9]

Sources of geometric distortion in MR images are either system-related (gradient field non-linearity and B_0 inhomogeneity) or patient-induced (chemical shift and susceptibility differences).[3,10–12] Alternatively, they can be grouped into sequence dependent and sequence independent,[13,14] based on specific distortion characteristics. In particular, B_0 inhomogeneity, chemical shift effects and susceptibility differences are collectively referred to as sequence dependent or field distortions, as geometric distortion direction depends, by definition, on read gradient polarity.[13,15,16] More specifically, a change in the polarity of the frequency encoding gradient (i.e., read gradient) will result in sequence dependent distortion of the same magnitude but opposite sign. Moreover, in conventional, three-dimensional (3D) non echo planar imaging (EPI) sequences, image warping mainly occurs in the frequency encoding axis (i.e., read gradient direction). On the other hand, gradient field non-linearity can induce considerable geometric distortion on all three axes, while the sign of distortion is not affected by read gradient polarity reversal (i.e., sequence independent distortion).[13]

Scanner manufacturers have developed and implemented post-imaging distortion correction routines that minimize gradient non-linearity related effects. Nevertheless, residual distortion may be significant at any direction, especially at areas distant from the MR isocenter.[3] As an instance, a 0.5 mm average distortion magnitude was revealed for a brain scan for SRS applications with maximum detected offset exceeding 1 mm at the edges of the field-of-view[12] and is therefore comparable to typical sequence dependent distortion levels.[3,11] Since sequence

independent spatial distortion does not relate to the patient being scanned, it can be measured a priori using specially designed phantoms[12,16–19] and corrected for in clinical examinations. Contrarily, sequence dependent distortion cannot be evaluated and corrected beforehand. Sequence dependent distortion may also exceed 1 mm mainly on the frequency encoding direction and, therefore, may result in considerable target underdose, potentially compromising treatment efficiency.[8,9,11]

Two main approaches have been identified for the evaluation and correction of sequence dependent distortions. The first is based on the field mapping technique,[20] whilst the second on the read gradient polarity reversal method.[15] The former uses phase difference maps from a dual echo gradient echo pulse sequence while the latter exploits the fact that sequence dependent distortion changes sign (but not magnitude) upon read gradient polarity reversal. Although the above approaches have been repeatedly used for distortion evaluation,[11–14,16,21–23] studies reporting on patient specific distortion correction are limited[8,13,24–27] with only a few focusing on cranial cases. Morgan et al.[24] proposed the signal integration (SI) method, exploiting the fact that the integrated signal along the frequency encoding axis remains unaffected in both the forward and reversed read gradient polarity images. Karaiskos et al.[8] employed the "mean image" (MI) approach, based on averaging the signal on a pixel-by-pixel basis from the corresponding forward and reversed polarity images. Other groups directly acquired phase difference maps using the field mapping (FM) technique and calculated distortion maps.[23,26] Technical details for the FM, MI and SI techniques are given in section 2.A.4. However, none of the above distortion correction schemes has been widely adopted in clinical practice. Moreover, with the exception of one work,[8] previous studies have not focused on the distortion at the lesion location(s) which directly affects target localization and delineation accuracy, especially in SRS treatment planning.

In the present study, we utilize three patient specific distortion correction schemes (SI, MI and FM) and evaluate their accuracy and efficiency at the lesion locations for SRS treatments of single or multiple brain metastases. To this purpose, a comprehensive QA methodology, comprising an anthropomorphic head phantom (filled with polymer gel dosimeter) and appropriate algorithms and workflows, was developed and implemented. In the phantom study, the performance of all three correction methods was evaluated in terms of residual geometric offset between the polymerized centroids, which served as hypothetical metastases. To evaluate the correction efficiency under clinical conditions (i.e., at real target locations), a patient study was also performed. The same correction schemes were applied to contrast enhanced T1w MR images

of 10 patients with a total of 27 brain metastases, used for SRS treatment planning purposes. Correction efficacy, practicability and limitations of each correction scheme are assessed, discussed and inter-compared.

2. MATERIALS AND METHODS

2.A. Phantom study

2.A.1. Phantom description

A commercially available head phantom (RTsafe P.C., Athens, Greece), 3D-printed based on real patient's planning CT images,[28] was utilized in this study [Fig. 1(a)]. In specific, the external shape as well as the CT-identified bony structures of a patient are 3D-printed using bone mimicking material.[28] Then, the hollow phantom is filled with a 3D polymer gel dosimeter, also acting as tissue equivalent material. Following treatment planning and dose delivery, the radiation-induced polymerization at high dose areas provides adequate signal contrast against the unirradiated "brain parenchyma" in both T1- and T2-weighted (T1w and T2w, respectively) MR images. Depending on the treatment plan (i.e., dose gradients and dose distribution delivered), radiation induced polymerized volumes simulating brain metastases can be created at any number, size, shape and location.

For the purposes of this study, four hypothetical brain lesions were planned for treatment in GammaPlan v.9 treatment planning system (TPS), as shown in Fig. 1(b). The phantom was mounted on the Leksell stereotactic frame and irradiated with four single-shot or multi-shot dose distributions using an Elekta Gamma Knife Perfexion unit (Elekta Instrument AB, Stockholm, Sweden). Thus, four polymerized volumes representing the treated lesions were created within the tissue equivalent gel volume simulating the brain parenchyma.[14] One large lesion (approx. volume 2900 mm^3) was prescribed towards the inferior phantom base, two lesions towards the central brain area (approx. volumes 490 and 1860 mm^3 respectively) and one (approx. volume 680 mm^3) towards the superior side, as illustrated in Figs. 1(b) and 1(c).

2.A.2. MRI scanning

All phantom scans were performed at 1.5 T (Multiva, Philips Medical Systems, The Netherlands), approximately 24 hours post irradiation, when radiation induced polymerization is considered to be mature enough and stable within the time interval of a scanning session.[29] A phased array head coil was used for signal reception. All sequences employed were 3D gradient

recalled echo (GRE) pulse sequences with enabled the 3D routine supplied by the vendor for gradient non-linearity correction. Scanning sequences and parameters employed, as well as image series acquired, are provided in Table I. Acquisition and reconstruction matrices were equal in size. Image series A1 (Table I) was obtained with the clinical protocol used for target localization in SRS procedures and, consequently, it corresponds to the uncorrected image set. The other three image series were acquired to implement the distortion correction methods under investigation.

2.A.3. Estimation of reference lesion locations

To evaluate the performance of each correction method, the reference location of each hypothetical lesion was determined, based on the well-established reversed read gradient polarity technique.[12–16] To implement this method, an additional scan is performed with exactly the same imaging parameters as the original one, apart from the read gradient polarity (image series A2, Table I). Since the polarity change affects only the sign of the sequence dependent distortion but not its magnitude, a pair of positions corresponding to a distinct point can be identified on the forward and reverse images.[12–14] The average position of the paired positions can be regarded as the respective reference location of the distinct point, as it is, by definition, free of sequence dependent distortion. Similar approaches have been repeatedly adopted in several distortion evaluation studies.[11–16]

MR images in DICOM format were analyzed using custom-made, in-house routines developed in MATLAB R2018b (The MathWorks, Inc., Natick, MA). All four hypothetical metastases were identified in the 3D image stacks, by exploiting the signal contrast between polymerized (i.e., high dose) and unpolymerized areas [Fig. 1(c)]. Binary images were obtained through semi-automatic contouring on the imported image series. In specific, an algorithm was developed to determine the most appropriate signal threshold, defining the volume of the lesion within a predefined region of interest. Emphasis was put on contouring to obtain similar volumes in the two image stacks, by slightly adjusting the threshold levels. In all phantom-related images, typical threshold levels were 1850 ± 50. Determined structures, representing targets, were manually reviewed and verified. This approach was adapted from a previous study.[11] The centroid of each structure volume in the DICOM coordinate system was estimated in the two scans, while the average centroid position served as the reference control point location for distortion evaluation,[11–16] as well as for characterizing the performance of the distortion correction techniques considered. Determined centroid locations were not sensitive to signal threshold

selection. Sequence dependent distortions at the target locations were calculated as the geometric offsets between reference locations and corresponding positions in the original image series (i.e., A1 and B1, Table I).

2.A.4. Correction methods

2.A.4.1. Field mapping technique

The FM technique,[13,20,22,30,31] which is routinely employed in periodic quality control procedures to evaluate the static magnetic field inhomogeneity,[31] can be used to evaluate and correct sequence dependent distortion.[13,20,22,30,31] Briefly, this method uses the phase maps acquired at two different echo times using GRE sequences. Phase difference maps can be determined, as a result of a post-processing phase unwrapping procedure, using in-house routines.[32] Field (i.e., sequence dependent) distortions are directly proportional to the magnetic field variations and can be obtained from the unwrapped phase difference map on a pixel-by-pixel basis.

The relevant imaging series are A3 and A4 (B3 and B4 for the patient study) in Table I. The echo times (TEs) used were carefully selected to avoid severe phase wrapping,[33] which could potentially compromise the method's efficacy. Phase difference maps were calculated and unwrapped in MATLAB R2018b, implementing a methodology described in Cusack and Papadakis,[32] using routines developed and validated for the purposes of a previous study.[11] Briefly, it is an iterative algorithm that uses the negated magnitude as the noise field estimator for 3D guided phase unwrapping and, therefore, areas suffering from increased noise are unwrapped last. Distortion maps (either in Hz or mm) are directly proportional to the unwrapped phase difference maps.[13,33] Undistorting the original, forward MR images (image series A1 or B1, Table I) requires a simple interpolation step between the distorted and undistorted image spaces.[13] In the undistorted image space, however, pixel intensities should also be corrected, as pixels also suffer from signal variation due to their compression or deformation in the distorted image space. In other words, spatial distribution of signal is different in distorted and undistorted image spaces. To compensate for this, a Jacobian determinant term, which can be easily calculated from the calculated distortion map,[13,25] was applied as proposed by Reinsberg et al.[25]

2.A.4.2. Mean image technique

The MI method was proposed by Karaiskos et al.[8] The technique exploits the fact that field distortions change sign upon read gradient polarity reversal. A mean image is created for each pair of forward and reversed polarity images. The signal intensity of each pixel in the corrected mean image is simply the mean pixel value of the two corresponding pixels in the two original images acquired with forward and reverse polarity of the read gradient.

Image processing of the acquired image series A1 and A2 (or B1 and B2 for the patient study, Table I) was performed in MATLAB R2018b. The technique is simple and efficient, with post-processing time of the order of 1 second.[8,34] It should be noted, however, that this method does not involve creation of distortion maps and, consequently, the signal intensity correction using the Jacobian determinant cannot be applied.

2.A.4.3. Signal integration technique

Morgan et al.[24] proposed another approach for distortion correction, also based on the read gradient reversal method. Acknowledging that the signal integral across a line along the frequency encoding axis remains unaffected by spatial distortion, matching points between the forward and the reversed polarity image stacks can be identified and paired at the locations where the two integrals equalize, thus yielding the distortion map.[24,34] A low signal cut-off threshold is applied in order to exclude voxels outside patient anatomy or of very low SNR, which could affect integration results. Following determination of the distortion map, image correction is a simple interpolation task. The Jacobian determinant can be used to correct for pixel intensity, as in the FM technique. Details on the implementation of the SI method can be found in the literature.[24,34] Specific to this study, the corrected image is generated from the combination of image series A1 and A2 (or B1 and B2 for the patient study, Table I). All necessary routines were developed in-house using MATLAB and have been validated in a previous phantom study.[34] However, the SI technique is associated with increased computational time (of the order of 1 hour) for deducing the corrected 3D image volume.

2.A.5. Residual distortion evaluation

Following application of the three distortion correction methods, all four hypothetical lesions were identified and semi-automatically contoured in each one of the three corrected image sets. The centroid of each polymerized volume was determined in the DICOM coordinate system using the MATLAB routines and methodology described in section 2.A.3 for the original,

distorted image series. Extracted centroids of the lesions in the corrected image volumes were compared against the corresponding reference locations (see section 2.A.3), yielding the residual sequence dependent distortion for each correction technique.

2.B. Patient study

A total of 10 patients with single or multiple brain metastases, treated with Gamma Knife stereotactic radiosurgery, were enrolled in the patient study of this work, approved by the institutional Ethics Committee. Patients were selected in order to include lesions varying in size, shape and location within the brain parenchyma, while patients with large (>4000 mm^3) lesions or lesions presenting necrotic core or indistinct borders were excluded. All MR images were acquired at 1.5T (Achieva, Philips Medical Systems, The Netherlands), implementing the institution's clinical protocol for SRS treatment planning. This involved the use of a stereotactic frame, ensuring patient immobilization during the entire scanning session, and an appropriate head coil. This setup also resulted in the MR isocenter being centered within the imaged volume, for all patients, irrespective of lesion location(s). Table II presents the physical characteristics of all 27 lesions studied. All images were contrast-enhanced following an intravenous injection of 0.2 mmol kg^{-1} gadolinium diethylenetriamine pentaacetic acid (Gd-DTPA).

The protocol included all the necessary clinical sequences, as well as the additional image acquisitions required to implement the three correction techniques considered in this study. Overall, scan parameters were similar to the ones employed in the phantom study (Table I, image series B1-B4), with minor changes to maintain sufficient signal-to-noise ratio (SNR) and tolerable scanning time, according to the clinical protocol. The selected bandwidth level provides adequate SNR even for the tiniest brain lesions.[11] Acquisition voxel size was 0.9×0.9×1.5 mm^3 for B1-B4 images.

Patient image analysis for distortion evaluation and correction followed the same methodology described in the phantom study (see section 2.A). Thus, images were exported in DICOM format and analyzed in MATLAB, using the same in-house routines. A total of 27 metastases were identified and semi-automatically contoured in the original forward and reverse image series (i.e., B1 and B2, Table I), as well as in the three undistorted image sets. A typical threshold value for lesion determination was typically around 600, but was slightly adjusted in order to obtain contours of similar volume in all image series. This was necessary in order to ensure that the contouring is not biased by increased or decreased signal or contrast in any of the

images involved. For instance, the reversed polarity image often exhibits slightly different signal levels within the lesions because it is acquired after the forward polarity MR scan and, therefore, contrast agent concentration within the lesion is changed. In all cases, obtained structures were manually reviewed and verified, in order to exclude false positives such as vessels (with contrast agent uptake) in the vicinity of lesions. Nevertheless, the corresponding centroids were treated as control points for distortion detection and performance evaluation of the undistorting techniques and it should be noted that lesion centroid locations were not sensitive to the threshold value selected. As in the phantom study, the average centroid location of a lesion identified in the forward and reversed polarity images served as the reference lesion location in the DICOM space (see section 2.A.3). Sequence dependent (also patient induced) distortion was estimated as the geometric offset between the reference lesion centroid and the corresponding centroid identified in the original image series acquired with forward read gradient polarity MR scan. The performance of the three correction methods employed was evaluated through the determination of the residual spatial distortion. To this purpose, lesion centroids identified in the corrected image sets were benchmarked against the corresponding reference locations.

3. RESULTS

3.A. Phantom study

Figure 2 summarizes the results of the phantom study. For each target considered, the original sequence dependent distortion on the frequency encoding axis (Anterior-Posterior direction), along with the residual distortions, following the application of each correction method, are provided. Original distortion magnitude was approximately 0.7 mm (2.10 ppm) (median: 0.7 mm, maximum: 0.8 mm) at all target locations. All three correction methods successfully reduced the corresponding offset to 0.2 mm (0.61 ppm) or less. Residual distortion in the FM method was systematically larger than the corresponding distortions related to the other two methods.

Figures 3(a)-(d) present the same axial slice of the original and corrected MR image volumes, intersecting the target planned towards the superior side of the phantom [see Figs. 1(b) and (c)]. Contours depict the target location as identified in the four images. To quantitatively compare target location, Fig. 3(e) presents corresponding signal intensity profiles along the frequency encoding direction. A sub-millimeter shift of the target signal distribution in the original (uncorrected) MR image is evident, while the profiles corresponding to the three corrected images are in agreement with each other [Fig. 3(e)].

A visual inspection of the corrected MR images suggests that image quality is acceptable, using any of the three correction methods [Figs. 3(b)-(d)]. For the SI corrected image [Fig. 3(d)], the effect of the low signal cut-off threshold is evident, nulling pixels of very low signal intensity (e.g., background noise or partial volume pixels). Other than that, any differences in the presented images are hardly visible. For comparison, Table III presents the calculated contrast-to-noise ratios (CNRs) for the images shown in Figs. 3(a)-(d). CNR was slightly increased in all corrected images.

3.B. Patient study

To evaluate the efficacy of the correction techniques in the clinical setting, the same approaches, routines and workflows were applied to images from patients referred for the treatment of single or multiple brain metastases. Corresponding results are summarized in Table IV. Regarding the original images (i.e., no correction applied), the measured sequence dependent distortion along the frequency encoding axis varied from lesion to lesion, with magnitude depending on the metastasis position, as well as on other physical characteristics (e.g., size, shape, adjacent tissues or contrast agent uptake[11]). For the 27 metastases studied, the original distortion magnitude lied in the 0.09 – 0.75 mm (0.36 – 3.09 ppm) range, with median distortion being 0.42 mm (1.75 ppm). Following application of any of the three distortion correction routines, median distortion magnitude on the frequency encoding axis was reduced by a factor of at least 2.6 (Table IV), although maximum residual distortion in the FM corrected images was 0.55 mm (2.29 ppm). The MI correction method was the most effective, with corresponding median and maximum residual distortion magnitudes being 0.07 mm (0.31 ppm) and 0.24 mm (0.99 ppm), respectively.

In order to illustrate the spread of original and residual distortion measurements, Fig. 4 presents the patient study results in box-whisker plots. Original sequence dependent distortion in the uncorrected MR images covers a range of 0.66 mm. Although all three correction methods successfully minimize median distortion magnitude, results for the FM technique cover a 0.55 mm range. On the other hand, the MI approach provides more consistent results (0.24 mm range), appearing to be the least affected technique by signal variations (e.g., stemming from physical and anatomical differences) in the vicinity of the lesions.

In an effort to visualize lesion shift as a result of the distortion correction procedure, Fig. 5 presents signal intensity profiles along the read gradient direction for the original and corrected

MR images of three metastases. All three correction techniques shift target positions with regard to the high signal intensity pixels (Fig. 5). Occurring target shifts are always sub-millimeter (i.e., sub-pixel), but still evident and always towards the same direction for each target among the three corrected images Fig. (5).

In order to demonstrate and compare image quality of the original and corrected images, Fig. 6 presents the same axial slice intersecting a brain lesion prior to (a) and after distortion correction (b-d). Image quality of the corrected images is acceptable in all cases, especially at the high intensity areas (Fig. 6). However, FM is characterized by increased random noise in the brain parenchyma [Fig. 6(b)]. The effect of the low signal cut-off threshold applied in the SI corrected image is evident, as structures of very low signal intensity or partial volume pixels are nulled [Fig. 6(d)].

For the slices shown in Fig. 6, Table V presents CNR measurements between the central target area and a region of interest within the brain parenchyma, calculated as in the phantom study (see section 3.A). CNR was found to be considerably increased in all corrected images in relation to the original image.

4. DISCUSSION

Selection of a suitable phantom yielding MR signal and contrast and simultaneously simulating brain lesions is challenging. Several groups have employed plastic or acrylic-based phantoms filled with paramagnetic solution.[12,16,17,35,36] Although such phantoms can be easily constructed or are commercially available, plastic or acrylic does not yield MR signal. Thus, the hypothetical lesions are not depicted as increased signal areas superimposed on a lower signal background, as typically occurs in clinical brain images. In the phantom study of this work, increased T1w MR signal in pre-selected areas simulating four lesions spread throughout the brain parenchyma was produced by employing an anthropomorphic head phantom filled with a 3D polymer gel dosimeter and by irradiating the hypothetical lesions. This approach is suitable to evaluate the three correction methods under optimal conditions, i.e., of high signal contrast, without involving material inhomogeneities and susceptibility cavities commonly encountered in clinical images (such as air cavities or contrast enhanced blood vessels). Irradiating a polymer gel volume to create signal contrast in MR images is not an entirely new methodology. Moutsatsos et al. delivered 26 Gamma Knife shots (i.e., spherical dose distributions) in order to introduce control

points for distortion detection in T2w images for SRS applications.[14] In the current study, the same approach was followed, although acquired images were T1w using clinical pulse sequences and parameters while an anthropomorphic phantom was used instead of a generic spherical one. Volumes of radiation-induced polymerization correspond to areas of increased signal in T1w images, in contrast to the reduced signal obtained in T2w images.

From the implementation point of view, the MI method is the most straightforward with regard to developing all the necessary routines. No special processing steps are involved, while undistorting does not require interpolation. The technique is very simple as the only calculation step is pixel-wise averaging of the signal intensities in the paired images. The SI method is also a scheme relying on the read gradient polarity reversal. However, calculation of the signal integrals along the frequency encoding lines adds complexity to the image processing steps required, while undistorting relies on interpolation between the warped and unwarped image spaces. The FM method is typically employed in quality control procedures for the evaluation of the main magnetic field homogeneity,[31] using large phantoms. Thus, it can be expected that users are more familiar with it, although phase unwrapping may not always be a straightforward procedure. Furthermore, the FM technique only slightly increases the total acquisition time, in contrast to the methods employing the read gradient polarity reversal approach which burden the protocol with a particularly time-consuming pulse sequence.

All three methods demonstrated satisfying results in both phantom and patient studies. Image quality was not adversely affected, whilst CNR was increased. However, post-imaging process time differed greatly among correction schemes and significantly depends on the matrix size of the acquired images. The guided phase unwrapping step required in the FM method is time-consuming (approximately 1 hr),[13,32] while the SI technique needs a few hours of computational time.[34] The MI approach is by far the most efficient with post-processing time of the order of a few seconds.[8]

A number of limitations related to this study are noteworthy. First, simple routines were developed to implement each of the three correction techniques with conventional computer power. Specific implementation parameters and technical details were selected based on the experience of previous studies.[11,34] Although possibly sub-optimal, basic and easy-to-develop routines were found appropriate for the purposes of this study. However, more sophisticated routines can be developed, which could result in greatly reduced processing times for all three techniques. Performance of distortion correction approaches in areas other than the lesions was not

investigated. Potential target deformation due to considerable distortion gradient within the lesion(s) was not studied. In addition, 1D correction techniques were only applied and, therefore, target centroid displacement in the phase encoding axes, as a result of the image processing steps, was not evaluated. Moreover, susceptibility differences at tissue interfaces often induce increased spatial offsets.[10,37] However, lesions in close proximity to tissue inhomogeneities such as acoustic neuromas or lesions in the pituitary region were not considered herein. Metastases with necrotic cores, indistinct borderline or subtle enhancement were also excluded from the patient study. Furthermore, phantom and patient images studied did not involve any cases of severe original distortion (e.g., >1 mm) at the lesion locations. Investigating the efficacy of these techniques in heavily distorted images could be of particular interest. However, we focused on cranial images which are of limited field-of-view and used clinical imaging parameters to intercept realistic distortion magnitudes in cranial SRS applications. Increased distortions are commonly encountered in extracranial images employing larger field of views.[13] This also holds true for 3T MR images,[3] which were not included in the present study. As MR images were a priori considered spatially co-registered, gross patient motion in-between and during the MRI acquisitions could have been catastrophic for the efficacy of any distortion correction technique. In this work, a stereotactic frame (source of the extra-axial artefacts seen in Figs. 5 and 6) was used for patient immobilization throughout the rather prolonged MR imaging sessions. Performing MRI scans for SRS procedures with other or no immobilization apparatus is not uncommon. Potential intra-session patient motion during MRI scanning could lead to erroneous distortion correction. Thus, results of this study should only be considered valid under the scanning and immobilization conditions described herein and for cases with similar clinical and physical characteristics. Employment of other sequences and imaging parameters, contrast agent concentrations, field strengths and immobilization approaches could affect the performance of each correction scheme.

Overall, this work demonstrates that patient specific correction of MR-related distortion, focusing at the lesion location(s), is feasible. Although most often sub-millimeter, sequence dependent distortions directly affect target localization accuracy. Considering the increased dose gradients and target conformality in SRS procedures, the smaller the lesion volume the more susceptible to underdosage due to MR distortions,[8,9] let alone the increased dose to the normal brain parenchyma.[9] This could be exacerbated if sequence depended distortions are added up to other spatial uncertainties related to (i) gradient non-linearity distortion which is comparable in magnitude,[12] (ii) MR/CT registration[38] and (iii) patient positioning,[39] or to uncertainties associated

with (iv) the mechanical parts of the treatment delivery unit.[40,41] Although implementation of patient specific distortion correction schemes could potentially increase target localization in SRS treatment planning, stringent QA procedures need to be performed for their evaluation prior to integrating them into clinical practice. Towards this direction, an anthropomorphic polymer gel phantom (yielding realistic MR signal and contrast), as well as a suitable methodology and workflow focusing on SRS of brain metastases, were developed and presented in this study. Future work investigating necessity and applicability of correction schemes in other intracranial SRS cases, such as acoustic neuromas and lesions in the pituitary region, is warranted, whilst extracranial cases have also to be considered.

5. CONCLUSIONS

A phantom-based QA methodology for the evaluation of sequence dependent (also patient induced) distortion at the lesion location(s) was developed and implemented. The same workflow can also be applied to patient cranial MRIs. The main advantage of the presented QA methodology is that it focuses at the lesion location(s) where steep dose gradients are typically applied in SRS treatment planning.

The methodology was implemented to evaluate and compare three distortion correction techniques in both phantom and patient images. All correction schemes demonstrated promising results, minimizing the distortion of the original images which often exceeded 0.7 mm. Image quality was acceptable in all corrected images, while CNR was considerably increased. The MI technique appears to be the most efficient and requires minimum image processing and computational time, though patient scanning time is doubled.

Overall results of this work suggest that patient specific distortion correction at the lesion location(s) is feasible. However, prior to adopting a distortion correction workflow in clinical practice, a QA methodology needs to be established and validated.

Acknowledgments

This research is co-financed by Greece and the European Union (European Social Fund-ESF) through the Operational Programme «Human Resources Development, Education and Lifelong Learning» in the context of the project “Strengthening Human Resources Research

Potential via Doctorate Research" (MIS-5000432), implemented by the State Scholarships Foundation (IKY).

Conflict of Interest Statement

The authors have no relevant conflicts of interest to disclose.

References

1. Schmidt MA, Payne GS. Radiotherapy planning using MRI. *Phys Med Biol*. 2015;60(22):R323-R361. doi:10.1088/0031-9155/60/22/R323
2. Owrangi AM, Greer PB, Glide-Hurst CK. MRI-only treatment planning: benefits and challenges. *Phys Med Biol*. 2018;63(5):05TR01. doi:10.1088/1361-6560/aaaca4
3. Weygand J, Fuller CD, Ibbott GS, et al. Spatial precision in magnetic resonance imaging-guided radiation therapy: The role of geometric distortion. *Int J Radiat Oncol Biol Phys*. 2016;95(4):1304-1316. doi:10.1016/j.ijrobp.2016.02.059
4. Ma L, Sahgal A, Larson DA, et al. Impact of millimeter-level margins on peripheral normal brain sparing for gamma knife radiosurgery. *Int J Radiat Oncol Biol Phys*. 2014;89(1):206-213. doi:10.1016/j.ijrobp.2014.01.011
5. Nataf F, Schlienger M, Liu Z, et al. Radiosurgery With or Without A 2-mm Margin for 93 Single Brain Metastases. *Int J Radiat Oncol Biol Phys*. 2008;70(3):766-772. doi:10.1016/j.ijrobp.2007.11.002
6. Kirkpatrick JP, Wang Z, Sampson JH, et al. Defining the optimal planning target volume in image-guided stereotactic radiosurgery of brain metastases: Results of a randomized trial. *Int J Radiat Oncol Biol Phys*. 2015;91(1):100-108. doi:10.1016/j.ijrobp.2014.09.004
7. Seibert TM, White NS, Kim GY, et al. Distortion inherent to magnetic resonance imaging can lead to geometric miss in radiosurgery planning. *Pract Radiat Oncol*. 2016;6(6):e319-e328. doi:10.1016/j.prro.2016.05.008
8. Karaiskos P, Moutsatsos A, Pappas E, et al. A simple and efficient methodology to improve geometric accuracy in gamma knife radiation surgery: Implementation in multiple brain metastases. *Int J Radiat Oncol Biol Phys*. 2014;90(5):1234-1241. doi:10.1016/j.ijrobp.2014.08.349
9. Pappas EP, Alshanqity M, Moutsatsos A, et al. MRI-Related Geometric Distortions in

Stereotactic Radiotherapy Treatment Planning: Evaluation and Dosimetric Impact. *Technol Cancer Res Treat*. 2017;16(6):1120-1129. doi:10.1177/1533034617735454

10. Stanescu T, Wachowicz K, Jaffray DA. Characterization of tissue magnetic susceptibility-induced distortions for MRIgRT. *Med Phys*. 2012;39(12):7185-7193. doi:10.1118/1.4764481
11. Pappas EP, Seimenis I, Dellios D, Kollias G, Lampropoulos KI, Karaiskos P. Assessment of sequence dependent geometric distortion in contrast-enhanced MR images employed in stereotactic radiosurgery treatment planning. *Phys Med Biol*. 2018;63(13). doi:10.1088/1361-6560/aac7bf
12. Pappas EP, Seimenis I, Moutsatsos A, Georgiou E, Nomikos P, Karaiskos P. Characterization of system-related geometric distortions in MR images employed in Gamma Knife radiosurgery applications. *Phys Med Biol*. 2016;61(19):6993-7011. doi:10.1088/0031-9155/61/19/6993
13. Baldwin LLN, Wachowicz K, Fallone BG. A two-step scheme for distortion rectification of magnetic resonance images. *Med Phys*. 2009;36(9):3917. doi:10.1118/1.3180107
14. Moutsatsos A, Karaiskos P, Petrokokkinos L, et al. Assessment and characterization of the total geometric uncertainty in Gamma Knife radiosurgery using polymer gels. *Med Phys*. 2013;40(3):031704. doi:10.1118/1.4789922
15. Chang H, Fitzpatrick JM. A technique for accurate magnetic resonance imaging in the presence of field inhomogeneities. *IEEE Trans Med Imaging*. 1992;11(3):319-329. doi:10.1109/42.158935
16. Baldwin LLN, Wachowicz K, Thomas SDS, Rivest R, Fallone BG. Characterization, prediction, and correction of geometric distortion in 3 T MR images. *Med Phys*. 2007;34(2):388. doi:10.1118/1.2402331
17. Damyanovich AZ, Rieker M, Zhang B, Bissonnette J-P, Jaffray DA. Design and implementation of a 3D-MR/CT geometric image distortion phantom/analysis system for stereotactic radiosurgery. *Phys Med Biol*. March 2018. doi:10.1088/1361-6560/aab33e
18. Caramanos Z, Fonov VS, Francis SJ, et al. Gradient distortions in MRI: Characterizing and correcting for their effects on SIENA-generated measures of brain volume change. *Neuroimage*. 2010;49(2):1601-1611. doi:10.1016/j.neuroimage.2009.08.008
19. Tadic T, Jaffray DA, Stanescu T. Harmonic analysis for the characterization and correction of geometric distortion in MRI. *Med Phys*. 2014;41(11):112303. doi:10.1118/1.4898582

20. Jezzard P, Balaban RS. Correction for geometric distortion in echo planar images from B0 field variations. *Magn Reson Med*. 1995;34(1):65-73. doi:10.1002/mrm.1910340111
21. Huang KC, Cao Y, Baharom U, Balter JM. Phantom-based characterization of distortion on a magnetic resonance imaging simulator for radiation oncology. *Phys Med Biol*. 2016;61(2):774-790. doi:10.1088/0031-9155/61/2/774
22. Wang H, Balter J, Cao Y. Patient-induced susceptibility effect on geometric distortion of clinical brain MRI for radiation treatment planning on a 3T scanner. *Phys Med Biol*. 2013;58(3):465-477. doi:10.1088/0031-9155/58/3/465
23. Crijns SPM, Raaymakers BW, Lagendijk JJW. Real-time correction of magnetic field inhomogeneity-induced image distortions for MRI-guided conventional and proton radiotherapy. *Phys Med Biol*. 2011;56(1):289-297. doi:10.1088/0031-9155/56/1/017
24. Morgan PS, Bowtell RW, McIntyre DJO, Worthington BS. Correction of spatial distortion in EPI due to inhomogeneous static magnetic fields using the reversed gradient method. *J Magn Reson Imaging*. 2004;19(4):499-507. doi:10.1002/jmri.20032
25. Reinsberg SA, Doran SJ, Charles-Edwards EM, Leach MO. A complete distortion correction for MR images: II. Rectification of static-field inhomogeneities by similarity-based profile mapping. *Phys Med Biol*. 2005;50(11):2651-2661. doi:10.1088/0031-9155/50/11/014
26. Bagherimofidi SM, Yang CC, Rey-Dios R, Kanakamedala MR, Fatemi A. Evaluating the accuracy of geometrical distortion correction of magnetic resonance images for use in intracranial brain tumor radiotherapy. *Reports Pract Oncol Radiother*. 2019. doi:10.1016/j.rpor.2019.09.011
27. Crijns SPM, Kok JGM, Lagendijk JJW, Raaymakers BW. Towards MRI-guided linear accelerator control: Gating on an MRI accelerator. *Phys Med Biol*. 2011;56(15):4815-4825. doi:10.1088/0031-9155/56/15/012
28. Makris DN, Pappas EP, Zoros E, et al. Characterization of a novel 3D printed patient specific phantom for quality assurance in cranial stereotactic radiosurgery applications. *Phys Med Biol*. 2019;64(10):105009. doi:10.1088/1361-6560/ab1758
29. Papoutsaki M-V, Maris TG, Pappas E, Papadakis AE, Damilakis J. Dosimetric characteristics of a new polymer gel and their dependence on post-preparation and post-irradiation time: Effect on X-ray beam profile measurements. *Phys Medica*. 2013;29(5):453-460. doi:10.1016/j.ejmp.2013.01.003

30. Cusack R, Brett M, Osswald K. An Evaluation of the Use of Magnetic Field Maps to Undistort Echo-Planar Images. *Neuroimage*. 2003;18(1):127-142. doi:10.1006/nimg.2002.1281
31. Jackson EF, Bronskill MJ, Drost DJ, Och J, Sobol WT, Clarke GD. *AAPM Report No. 100 Acceptance Testing and Quality Assurance Procedures for Magnetic Resonance Imaging Facilities Report of MR Subcommittee Task Group 1*.; 2010. http://www.aapm.org/pubs/reports/RPT_100.pdf. Accessed December 11, 2017.
32. Cusack R, Papadakis N. New robust 3-D phase unwrapping algorithms: Application to magnetic field mapping and undistorting echoplanar images. *Neuroimage*. 2002;16(3 I):754-764. doi:10.1006/nimg.2002.1092
33. Holland D, Kuperman JM, Dale AM. Efficient correction of inhomogeneous static magnetic field-induced distortion in Echo Planar Imaging. *Neuroimage*. 2010;50(1):175-183. doi:10.1016/j.neuroimage.2009.11.044
34. Pappas EP, Dellios D, Seimenis I, Moutsatsos A, Georgiou E, Karaiskos P. Review and comparison of geometric distortion correction schemes in MR images used in stereotactic radiosurgery applications. *J Phys Conf Ser*. 2017;931(1):012031. doi:10.1088/1742-6596/931/1/012031
35. Stanescu T, Jans HS, Wachowicz K, Fallone BG. Investigation of a 3D system distortion correction method for MR images. *J Appl Clin Med Phys*. 2010;11(1). http://www.jacmp.org/index.php/jacmp/article/view/2961/1799. Accessed January 4, 2016.
36. Wang D, Doddrell D, Cowin G. A novel phantom and method for comprehensive 3-dimensional measurement and correction of geometric distortion in magnetic resonance imaging. *Magn Reson Imaging*. 2004;22(4):529-542. doi:10.1016/j.mri.2004.01.008
37. Adjeiwaah M, Bylund M, Lundman JA, Thellenberg Karlsson C, Jonsson JH, Nyholm T. Quantifying the effect of 3T MRI residual system and patient-induced susceptibility distortions on radiotherapy treatment planning for prostate cancer. *Int J Radiat Oncol*. 2017. doi:10.1016/j.ijrobp.2017.10.021
38. Ulin K, Urie MM, Cherlow JM. Results of a multi-institutional benchmark test for cranial CT/MR image registration. *Int J Radiat Oncol Biol Phys*. 2010;77(5):1584-1589. doi:10.1016/j.ijrobp.2009.10.017
39. Prentou G, Pappas EP, Logothetis A, et al. Dosimetric impact of rotational errors on the quality of VMAT - SRS for multiple brain metastases : Comparison between single - and

two - isocenter treatment planning techniques. *J Appl Clin Med Phys*. 2020;(October 2019):acm2.12815. doi:10.1002/acm2.12815

40. Poder J, Brown R, Porter H, Gupta R, Ralston A. Development of a dedicated phantom for multi-target single-isocentre stereotactic radiosurgery end to end testing. *J Appl Clin Med Phys*. 2018;19(6):99-108. doi:10.1002/acm2.12452
41. Brezovich IA, Popple RA, Duan J, et al. A novel phantom and procedure providing submillimeter accuracy in daily QA tests of accelerators used for stereotactic radiosurgery. *J Appl Clin Med Phys*. 2016;17(4):246-253. doi:10.1120/jacmp.v17i4.6295

LIST OF FIGURE CAPTIONS

Figure 1 caption:

FIG. 1. (a) The anthropomorphic gel-filled phantom with the Leksell stereotactic frame in position for CT scanning and treatment planning. (b) Axial (top) and sagittal (bottom) CT slices of the unirradiated phantom depicting the 10-Gy isodoses (yellow contours) corresponding to the four hypothetical brain lesions planned for treatment. (c) Axial (top) and sagittal (bottom) T1w MRI slices of the irradiated phantom, with radiation-induced polymerized areas appearing brighter than the unirradiated gel.

Figure 2 caption:

FIG. 2. Phantom study results. Histogram with the original and residual sequence dependent distortion magnitudes on the frequency encoding axis, at the four target locations. Abbreviations: FM: Field Mapping, MI: Mean Image SI: Signal Integration

Figure 3 caption:

FIG. 3. An indicative axial slice of the (a) original, (b) FM, (c) MI and (d) SI corrected T1w MR images, intersecting the target located towards the superior side of the phantom [see Figs. 1(b) and (c)]. On each image, four contours are superimposed depicting the target location, independently identified in each image stack (blue: original image, red: FM corrected image, orange: MI corrected image, green: SI corrected image). (e) Corresponding signal intensity profiles along the frequency encoding direction (Anterior-Posterior), centered at the assumed target.

Figure 4 caption:

FIG. 4. Box-whisker plots comparing the performance of the distortion correction methods implemented in the patient study. Red lines indicate median original or residual distortion magnitudes, whereas boxes range from the 1st to 3rd quartile. Whiskers depict the remaining data or extend up to 1.5 times the interquartile range in either direction. No outliers were detected in this dataset. Abbreviations: FM: Field mapping, MI: Mean image, SI: Signal integration.

Figure 5 caption:

FIG. 5. Axial slices (a, c, e) of the original T1w contrast enhanced MR images acquired for the patient study, intersecting three brain lesions. Each metastasis area is depicted magnified in the insert. For each target, the corresponding signal intensity profiles are given (b, d, f) along the red dashed line, parallel to the frequency encoding axis (Anterior-Posterior direction).

Figure 6 caption:

FIG. 6. Axial slices of the original (a), FM (b), MI (c) and SI (d) corrected, contrast enhanced T1w images intersecting the same brain lesion. In each image, the metastasis is depicted magnified in the corresponding insert.

TABLE I. Pulse sequences and main imaging parameters employed for the phantom and patient studies (image series A1-A4 and B1-B4, respectively).

Image series #	MRI pulse sequence	Receiver BW (Hz/pixel)	TE/TR/FA (ms/ms/°)	Read gradient axis / polarity	Voxel dimensions (mm3)	Acquisition time per 100 slices (min)
A1	T1w 3D spoiled GRE	192	4.6/25/30	y-axis / A-P	1×1×1	9.98
A2	T1w 3D spoiled GRE	192	4.6/25/30	y-axis / P-A	1×1×1	9.98
A3	1st echo 3D unspoiled GRE	155	4.4/14/30	y-axis / A-P	1×1×1	5.59
A4	2nd echo 3D unspoiled GRE	155	6.8/14/30	y-axis / A-P	1×1×1	5.59
B1	T1w 3D spoiled GRE	217	4.6/25/30	y-axis / A-P	0.82×0.82×1.5	9.58
B2	T1w 3D spoiled GRE	217	4.6/25/30	y-axis / P-A	0.82×0.82×1.5	9.58
B3	1st echo 3D unspoiled GRE	155	4.4/14/30	y-axis / A-P	0.82×0.82×1.5	5.32
B4	2nd echo 3D unspoiled GRE	155	6.8/14/30	y-axis / A-P	0.82×0.82×1.5	5.32

Abbreviations: BW: bandwidth, 3D: three dimensional, T1w: T1-weighted, GRE: gradient recalled echo, TE: echo time, TR: repetition time, FA: flip angle, A: anterior, P: posterior

TABLE II. Physical characteristics of the lesions included in the patient study.

Patient ID	No of metastases	Lesion volume		Max distance to MR isocenter (mm)
		Median (mm^3)	Range (mm^3)	
1	3	44.2	42.8 - 3950.2	78.8
2	3	108.3	37.1 – 619.5	69.6
3	1	1509.3	1509.3	68.6
4	2	56.6	43.0 – 70.2	54.2
5	2	39.6	23.0 – 56.3	88.5
6	3	40.3	19.4 – 313.9	101.2
7	3	61.3	18.6 – 89.6	59.4
8	3	42.8	32.7 – 43.4	52.1
9	4	26.9	24.2 – 30.5	91.1
10	3	46.6	22.4 – 164.4	89.4
Total	**27**	**45.4**	**18.6 – 3950.2**	**101.2**

TABLE III. Contrast to noise ratio (CNR) for the slices shown in Figs. 3(a)-(d), calculated using identical regions of interest in the unirradiated parenchyma and the central area of the irradiated target.

	No correction	**FM correction**	**MI correction**	**SI correction**
CNR $(S_t-S_p)/\sigma_p$	10.17	10.29	13.39	14.40

Abbreviations: S_t: the mean signal within a region of interest centered within the target, S_p and σ_p: mean and standard deviation, respectively, of the signal within a region of interest located in the parenchyma. FM: Field mapping, MI: Mean image, SI: Signal integration

TABLE IV. Patient study results. Original and residual sequence dependent distortion magnitude on the frequency encoding direction measured at the lesion locations.

Correction method	Min (mm / ppm)	Max (mm / ppm)	Median (mm / ppm)	Number of targets above 0.3 mm
No correction	0.09 / 0.36	0.75 / 3.09	0.42 / 1.75	20
FM correction	0.00 / 0.02	0.55 / 2.29	0.16 / 0.67	8
MI correction	0.00 / 0.00	0.24 / 0.99	0.07 / 0.31	0
SI correction	0.01 / 0.05	0.34 / 1.40	0.11 / 0.47	2

Abbreviations: FM: Field mapping, MI: Mean image, SI: Signal integration

TABLE V. Contrast to noise ratio (CNR) measurements for the slices shown in Fig. 6, using identical regions of interest in the brain parenchyma and the central area of the target.

	No correction	**FM correction**	**MI correction**	**SI correction**
CNR $(S_t-S_p)/\sigma_p$	19.58	20.87	22.47	23.14

Abbreviations: S_t: the mean signal within a region of interest centered within the target, S_p and σ_p: mean and standard deviation, respectively, of the signal within a region of interest located in the parenchyma. FM: Field mapping, MI: Mean image, SI: Signal integration

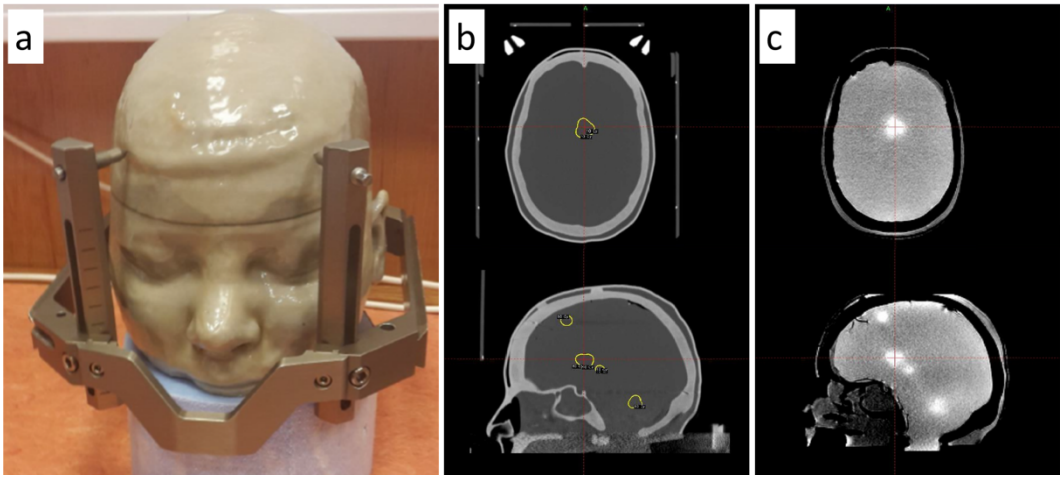

mp_14615_f1.tif

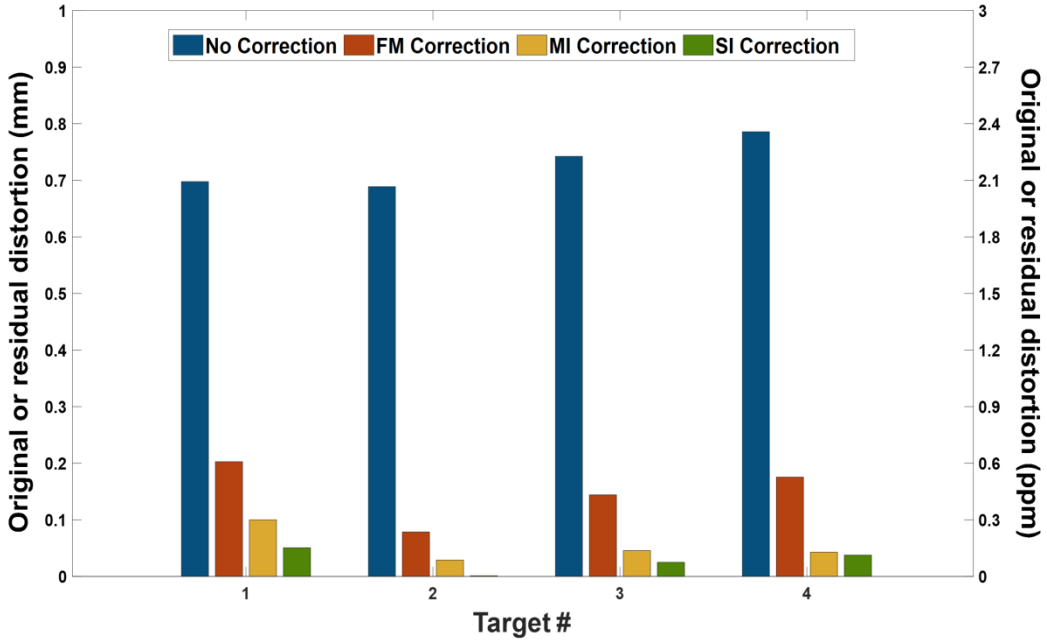

mp_14615_f2.tif

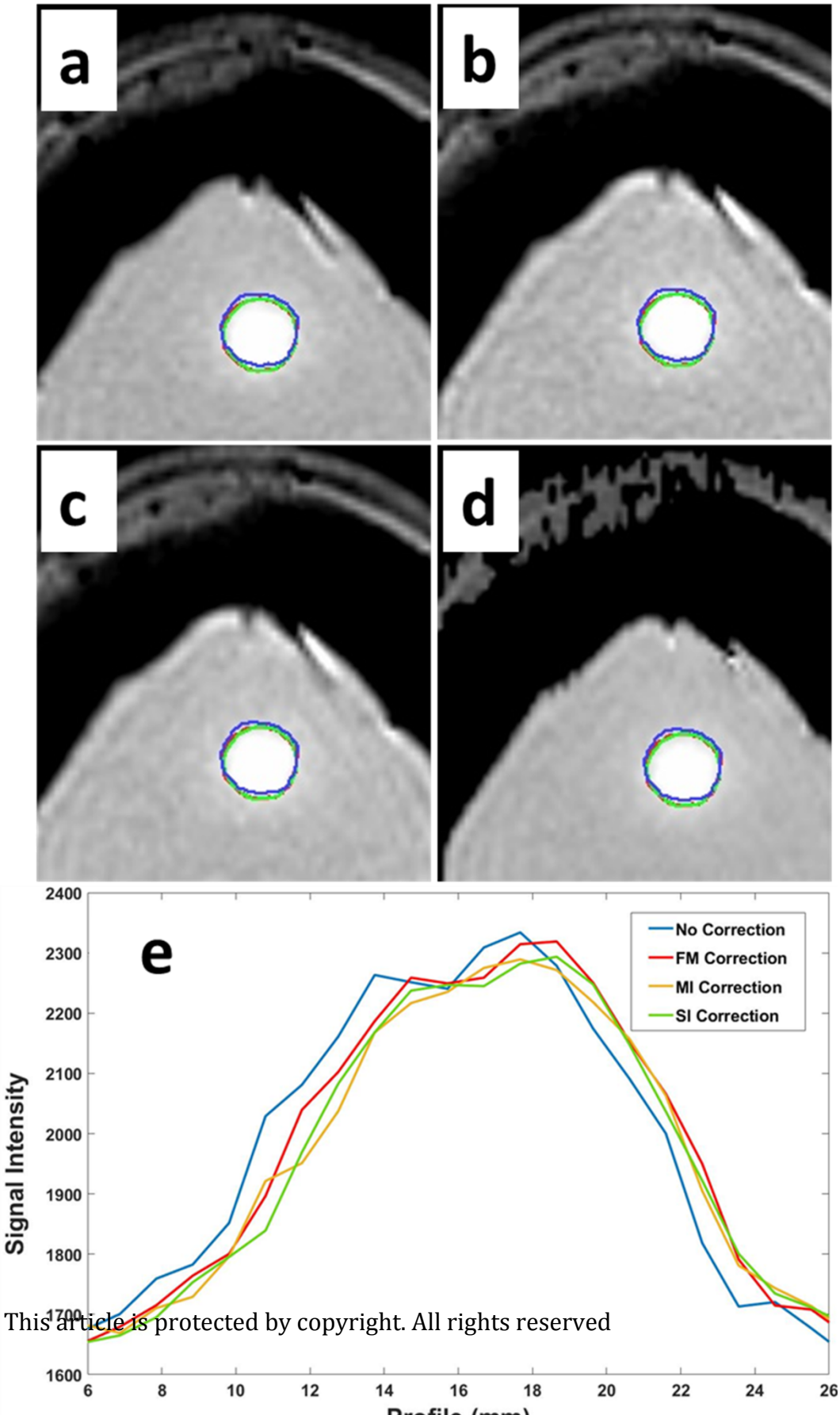

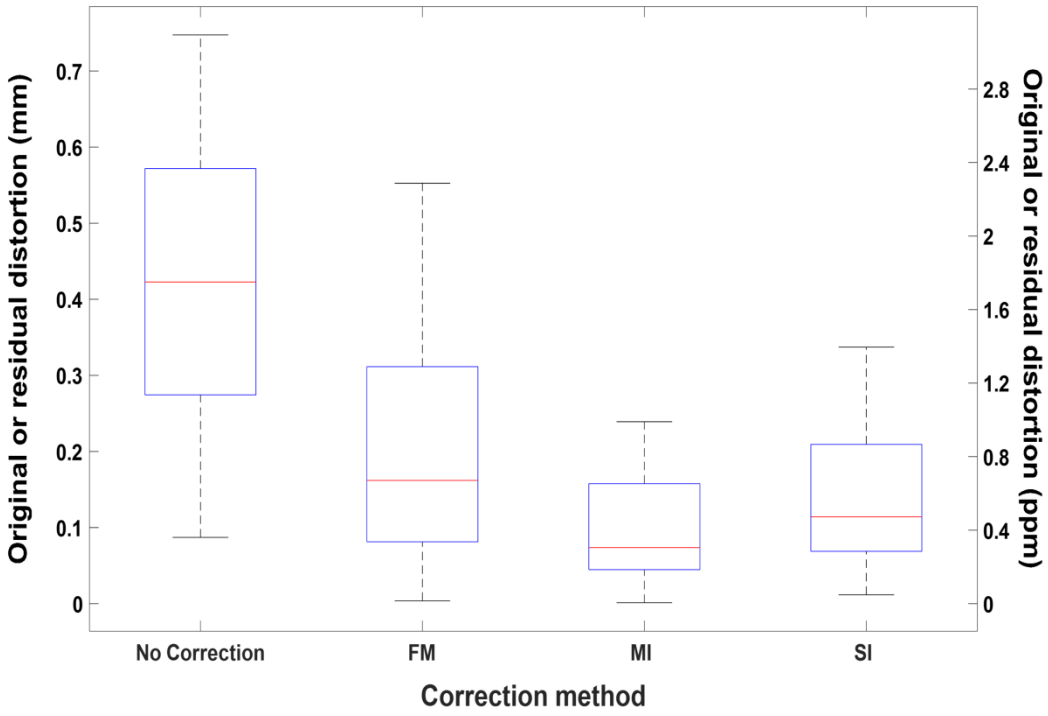

mp_14615_f4.tif

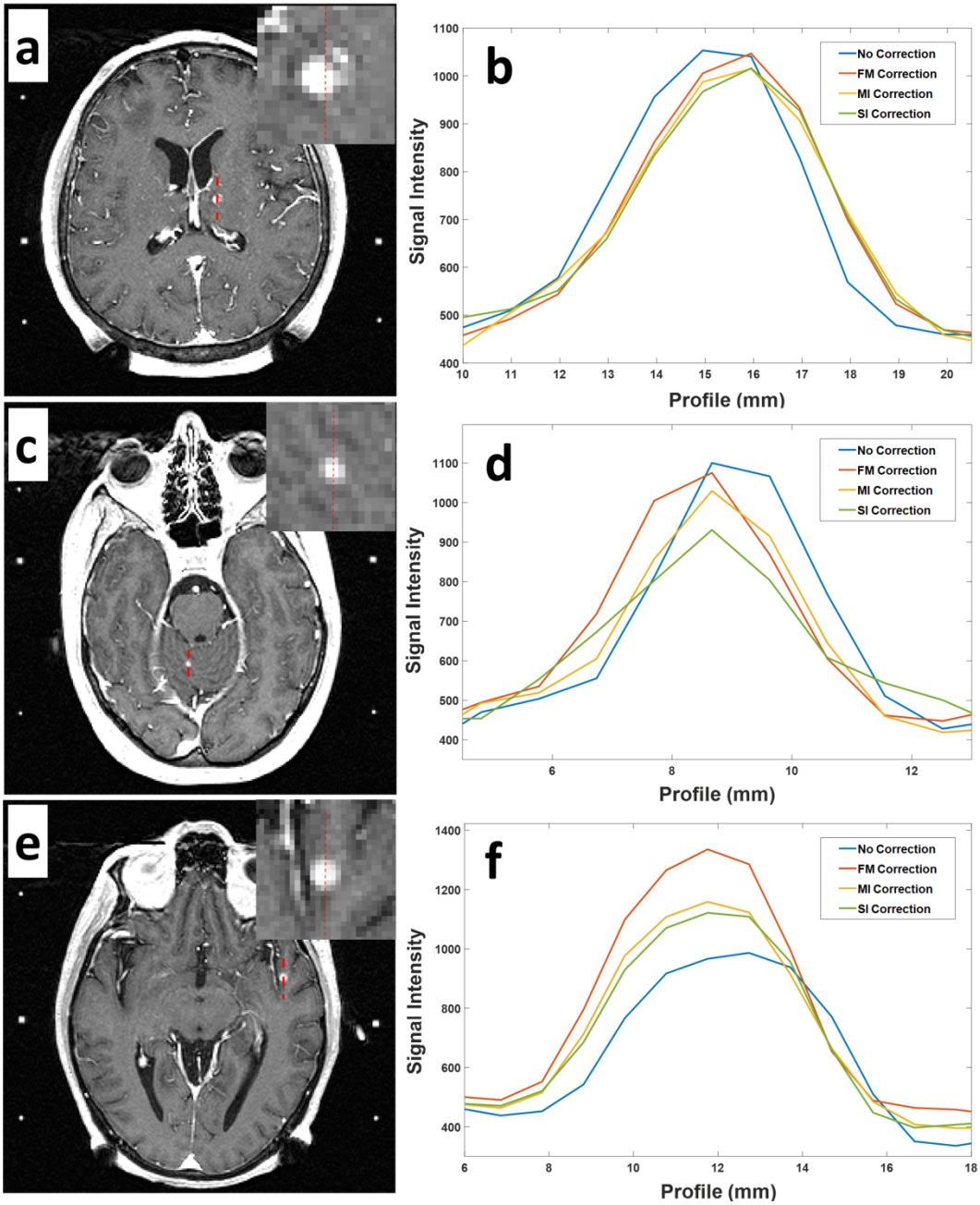

mp_14615_f5.tif

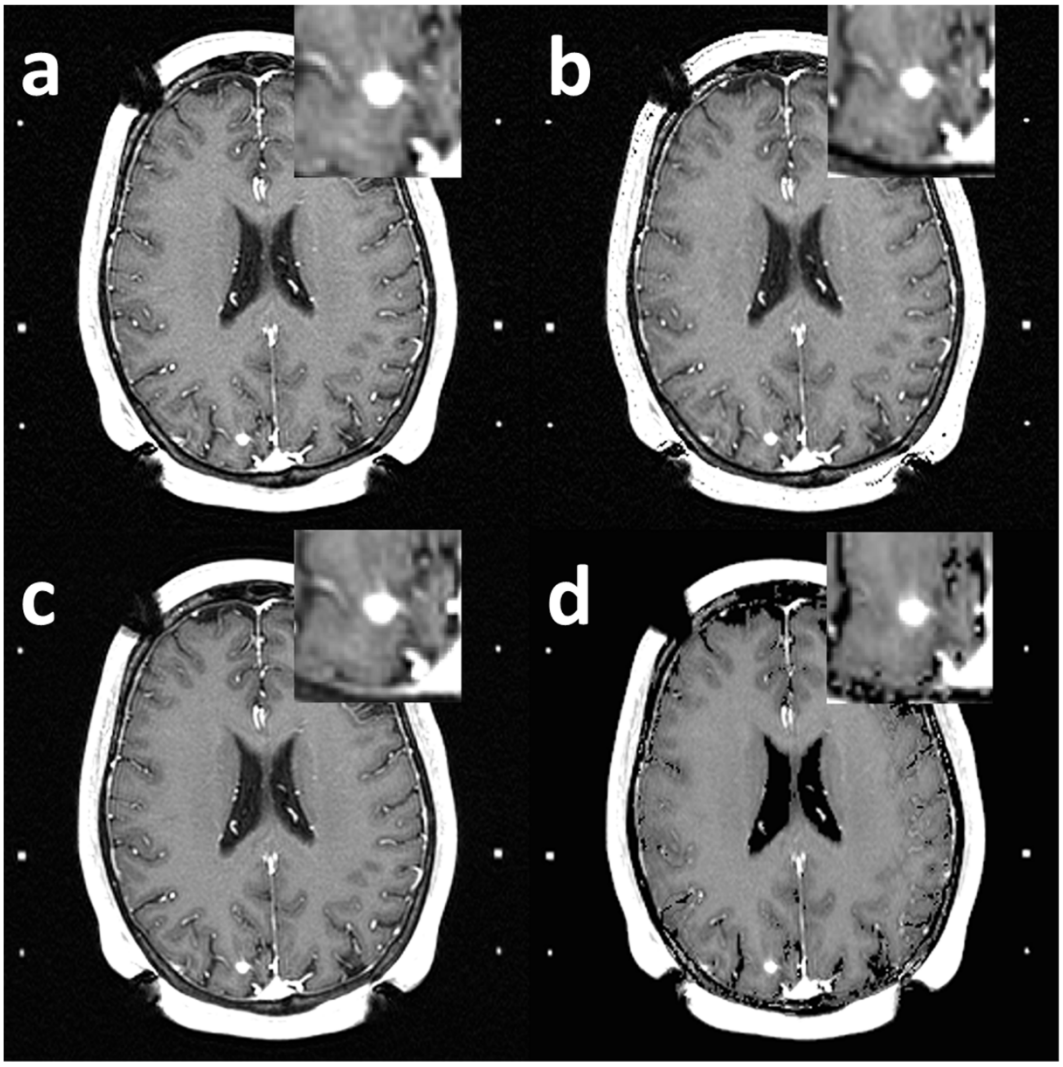

mp_14615_f6.tif